Quantum liquids in confinement: the microscopic view

2003 J. Phys.: Condens. Matter 15 S95

(http://iopscience.iop.org/0953-8984/15/1/311)

INSTITUTE OF PHYSICS PUBLISHING JOURNAL OF PHYSICS: CONDENSED MATTER

J. Phys.: Condens. Matter **15** (2003) S95–S100 PII: S0953-8984(03)54571-4

Quantum liquids in confinement: the microscopic view

E Krotscheck[1,2], V Apaja[1], A Rimnac[1] and R Zillich[3]

[1] Institute for Theoretical Physics, Johannes Kepler Universität, A-4040 Linz, Austria
[2] Institute for Nuclear Theory, University of Washington, Seattle, WA 98195, USA
[3] Department of Chemistry, University of California, Berkeley, CA 94720, USA

Received 9 October 2002
Published 16 December 2002
Online at stacks.iop.org/JPhysCM/15/S95

Abstract

We discuss, on a microscopic level, the effects of confinement on structural as well as dynamic properties of quantum liquids. The most evident *structural* consequences of confinement are *layer structures* found in liquid films, and *free surfaces* appearing in liquid drops and slabs. These structural properties have immediate consequences: new types of excitation such as surface phonons, layer phonons, layer rotons, and standing waves can appear and are potentially observable in neutron scattering spectra as well as in thermodynamic properties.

Atom scattering experiments provide further insights into structural properties. Methods have been developed to describe elastic and inelastic atom scattering as well as transport currents. The theory has been applied to examine scattering processes of ^{4}He and ^{3}He atoms impinging on ^{4}He clusters, as well as ^{4}He scattering off ^{4}He films and slabs.

1. Introduction

The effects of confinement have been a central topic in the research on quantum liquids over the past two decades [1], because confined systems provide more insights into the microscopic nature of the many-particle system than the bulk liquid. Confinement can be caused by external forces: quantum liquids in external matrices such as cavities, aerogels, hectorite gaps, or nano-tubes. Liquids can also be spontaneously 'confined' by the very nature of the many-particle Hamiltonian which makes the system self-bound. Quantum liquid clusters or slabs are examples. Finally, we have combinations of both effects, as in adsorbed liquid films. Variants of all of these systems are *mixed* configurations consisting, e.g. of ^{4}He and ^{3}He or ^{4}He with atomic impurities.

The structural properties of confined bosonic quantum fluids are quite well understood from no other information than an underlying Hamiltonian. Fermi fluids are technically significantly more tedious to deal with, but do not constitute a problem *in principle*. The theoretical method of choice for determining the structure of bosonic quantum fluids is Monte Carlo simulation which, however, becomes quite demanding when statistical fluctuations become an issue. In these situations, the Jastrow–Feenberg theory for inhomogeneous

systems [2] has turned out to be the optimal compromise between predictive power, technical effort, and minimal phenomenological input.

The description of the ground state of a many-boson system starts with the choice of a phenomenological Hamiltonian,

$$H_N = \sum_{i=1}^{N}\left[-\frac{\hbar^2}{2m}\nabla_i^2 + U_{\rm ext}(\boldsymbol{r}_i)\right] + \sum_{i<j} V(|\boldsymbol{r}_i - \boldsymbol{r}_j|). \tag{1}$$

Symmetry breaking may be induced by an external 'substrate' potential $U_{\rm ext}(\boldsymbol{r}_i)$, but it may also occur spontaneously like in the formation of quantum liquid droplets. For the wavefunction, one uses the Feenberg trial wavefunction,

$$\Psi_N(\boldsymbol{r}_1,\ldots,\boldsymbol{r}_N) = \exp\tfrac{1}{2}\left[\sum_i u_1(\boldsymbol{r}_i) + \sum_{i<j} u_2(\boldsymbol{r}_i,\boldsymbol{r}_j) + \sum_{i<j<k} u_3(\boldsymbol{r}_i,\boldsymbol{r}_j,\boldsymbol{r}_k)\right], \tag{2}$$

and determines the correlations by functional minimization of the energy expectation value. This requires, of course, the evaluation of the energy in an approximation that is consistent with the resulting Euler–Lagrange (EL) equations; the theory is known as the *optimized hypernetted-chain* (HNC-EL) theory. A feature that is particularly relevant for the problem at hand is that the functional optimization does not have a solution if the physical system is unstable against infinitesimal perturbations.

2. Structure

Typical systems are adsorbed films, liquid clusters, and slabs; a variant of adsorbed films is helium in aerogels and filled hectorite gaps where the liquid does not have a free surface. Common to all helium systems on a substrate is a layered structure of the liquid, and the effect of *layering transitions* [3, 4]. Translationally invariant systems cannot be found for all densities; rather, one finds sequences of translationally invariant and patched configurations [3], or abrupt transitions between systems of different numbers of atomic layers [4].

The prototype of systems that are confined due to many-body effects alone without any external potential are quantum liquid clusters; these can be produced and examined from a few atoms up to tens of thousands. Small clusters are of particular interest, because they display finite-size effects, and because comparisons between Monte Carlo simulations [5] and HNC-EL results [2] are available.

3. Dynamics

Dynamic situations are described by perturbing the system by a small, time-dependent potential that drives the system out of its ground state. All correlations in the Feenberg wavefunction (2) acquire time dependence and the excited state is

$$|\Psi(t)\rangle = \frac{\mathrm{e}^{-\mathrm{i}E_0 t/\hbar}\mathrm{e}^{\frac{1}{2}\delta U(t)}|\Psi_0\rangle}{[\langle\Psi_0|\mathrm{e}^{\mathrm{Re}\,\delta U(t)}|\Psi_0\rangle]^{1/2}}, \tag{3}$$

$$\delta U(t) = \sum_i \delta u_1(\boldsymbol{r}_i,t) + \sum_{i<j}\delta u_2(\boldsymbol{r}_i,\boldsymbol{r}_j,t) + \cdots \tag{4}$$

where $|\Psi_0\rangle$ is the ground state, E_0 the corresponding energy, and $U(t)$ is the time-dependent, complex *excitation operator*, which is determined by the action principle:

$$\delta\mathcal{S} = \delta\int_{t_0}^{t} \mathrm{d}t\,\langle\Psi(t)|H(t) - E_0 - \mathrm{i}\hbar\,\frac{\partial}{\partial t}|\Psi(t)\rangle = 0. \tag{5}$$

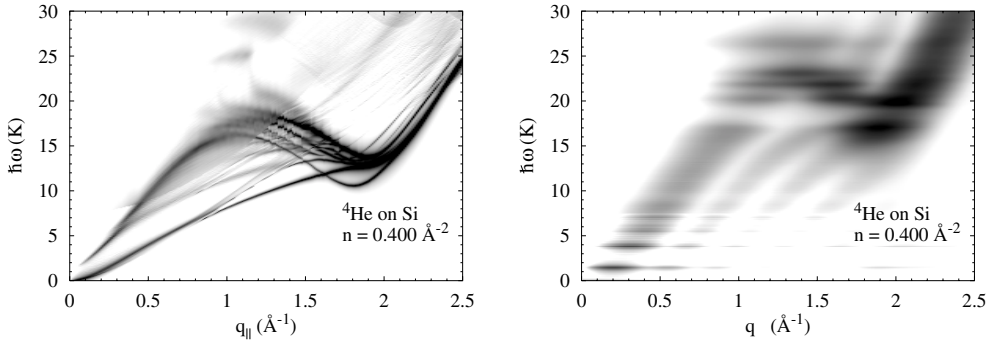

Figure 1. The figure shows the dynamic structure function $S(k, \omega)$ for a helium film with an areal density $n = 0.4$ Å^{-3} (nearly six liquid layers) adsorbed on silicon for momentum transfer *parallel* (left) and *perpendicular* (right) to the film.

The manipulations that lead to expressions for physical observables from equation (5) in an inhomogeneous geometry are somewhat lengthy [2], but they lead to a reasonably transparent form of the density–density response function:

$$\frac{\chi^{\mathrm{CBF}}(\boldsymbol{r}_1, \boldsymbol{r}_2; \omega)}{\sqrt{\rho_1(\boldsymbol{r}_1)}\sqrt{\rho_1(\boldsymbol{r}_2)}} = \sum_{m,n}[\phi_m^*(\boldsymbol{r}_1)[G_{mn}^{\mathrm{CBF}}(\omega) + G_{mn}^{\mathrm{CBF}}(-\omega)]\phi_n(\boldsymbol{r}_2)], \tag{6}$$

$$G_{mn}^{\mathrm{CBF}}(\omega) = [\hbar[\omega - \omega_m + \mathrm{i}\epsilon]\delta_{mn} + \Sigma_{mn}(\omega)]^{-1} \tag{7}$$

$$\Sigma_{st}^{\mathrm{CBF}}(\omega) = \frac{1}{2}\sum_{mn}\frac{\tilde{V}_{mn}^{(s)}\tilde{V}_{mn}^{(t)}}{\hbar(\omega_m + \omega_n - \omega)}. \tag{8}$$

The ω_m and $\phi_m(\boldsymbol{r})$ are the Feynman (or RPA) excitation energies and eigenfunctions, and $\tilde{V}_{mn}^{(t)}$ is a three-phonon coupling matrix element, which is neglected in the random phase approximation. The dynamic structure function $S(\boldsymbol{k}, \omega)$ is then obtained as Fourier components of the imaginary part of the density–density response function. The self-energy $\Sigma_{mn}(\omega)$ describes the interaction between single excitations in the host liquid. It is a non-local and non-Hermitian operator reflecting the fact that we are dealing with a system where a mode can either be absorbed or transfer some of its energy and momentum to other modes. In the three-phonon approximation, an excitation may decay into two excitations of lower energy.

Figure 1 shows a typical structure function for a helium film on graphite for parallel and for perpendicular scattering. In the *parallel* direction, we see two effects not present in the bulk liquid: one is a *surface mode* which has the typical $k^{3/2}$ dispersion relation. The second effect is a secondary roton minimum appearing below the energy of the bulk roton. Analysis of the relevant transition density reveals that this excitation corresponds to rotons propagating in the atomic layer closest to the substrate; hence these modes are called 'layer rotons'. In the perpendicular direction, we see a fragmented strength along the normal phonon–roton spectrum indicating a number of apparently dispersionless modes. These correspond to standing waves perpendicular to the surface; such modes have been seen in experiments on neutron scattering off ^{4}He adsorbed on graphite powder [6].

The dynamic structure function for droplets, shown in figure 2, displays fewer features. We still see the volume and surface modes, both broadened by finite-size effects; figure 2 also shows the density fluctuations induced by an incoming neutron beam at four different energies.

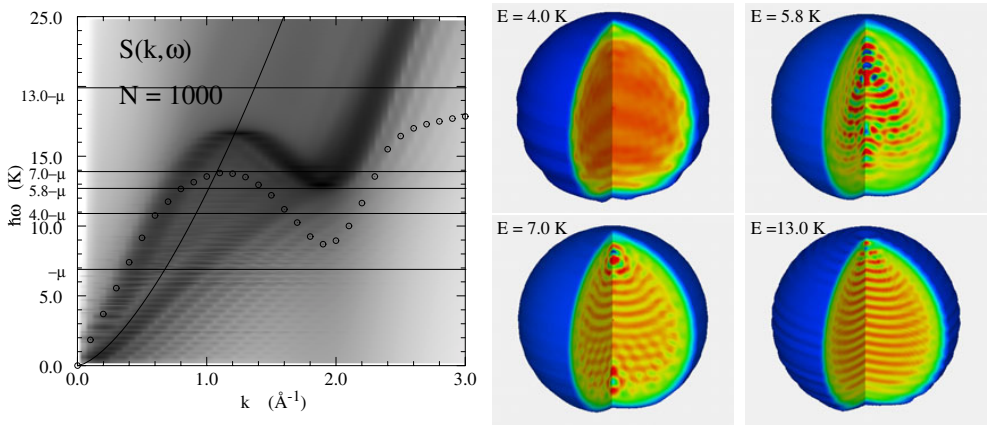

Figure 2. The left figure shows the dynamic structure function for a ^{4}He droplet with 1000 particles; the markers show the experimental phonon–roton spectrum. Note the ripplon and the phonon branches. The right figures show the density fluctuation induced in the droplet at the four different energies indicated in the left figure.

(This figure is in colour only in the electronic version)

4. Atom scattering

The continuum solutions of the effective Schrödinger equation

$$-\frac{\hbar^2}{2m}\left[\nabla^2 - \frac{\nabla^2\sqrt{\rho_1(\boldsymbol{r})}}{\sqrt{\rho_1(\boldsymbol{r})}}\right]\varphi_\omega(\boldsymbol{r}) + \int \mathrm{d}^3r'\,\Sigma(\boldsymbol{r},\boldsymbol{r}';\omega)\varphi_\omega(\boldsymbol{r}') = \hbar\omega\int \mathrm{d}^3r'\,S(\boldsymbol{r},\boldsymbol{r}')\varphi_\omega(\boldsymbol{r}') \quad (9)$$

describe the elastic channel of atom scattering. The equation of motion for impurity scattering is formally identical, except that the static structure function $S(\boldsymbol{r},\boldsymbol{r}')$ is replaced by $\delta(\boldsymbol{r}-\boldsymbol{r}')$.

The scattering solutions of equation (9) are delimited by the energy $\hbar\omega = -\mu + \hbar^2k^2/(2m)$, where the chemical potential is $\mu \approx -7$ K. $\Sigma(\boldsymbol{r},\boldsymbol{r}';\omega)$ is the configuration-space representation of $\Sigma_{mn}(\omega)$. The real part of the self-energy renormalizes the excitation energies and the imaginary part describes their finite lifetime.

The flux of outgoing atoms is given by the expectation value of the current operator $\hat{\boldsymbol{j}}(\boldsymbol{r})$ with respect to the wavefunction (3), calculated to *second order* in the fluctuating correlations $\delta U(t)$:

$$\boldsymbol{j}_2(\boldsymbol{r}) \equiv \frac{1}{4}\frac{\langle\Psi_0|\delta U^*(t)\,\hat{\boldsymbol{j}}(\boldsymbol{r})\,\delta U(t)|\Psi_0\rangle}{\langle\Psi_0|\Psi_0\rangle}. \quad (10)$$

The excitation operator $\delta U(t)$ is obtained from the *first-order* equations of motion (5).

The general second-order current is quite complicated, but only a few terms survive at large distances from the system. The three-phonon approximation to the equations of motion used in section 3 leads to tractable expressions for the second-order currents:

$$\begin{aligned}\boldsymbol{j}_2(\boldsymbol{r}) \to \mathrm{Re}\,\frac{\hbar}{4mi}\left[\varphi^*_\omega(\boldsymbol{r};t)\,\boldsymbol{\nabla}\varphi_\omega(\boldsymbol{r};t) + \int \mathrm{d}^3r_2\,\mathrm{d}^3r_3\,S(\boldsymbol{r}_2,\boldsymbol{r}_3)\,\delta\tilde{u}^*_2(\boldsymbol{r},\boldsymbol{r}_2)\,\boldsymbol{\nabla}_r\delta\tilde{u}_2(\boldsymbol{r},\boldsymbol{r}_3)\right] \\ \equiv \boldsymbol{j}_{2,\mathrm{el}}(\boldsymbol{r}) + \boldsymbol{j}_{2,\mathrm{inel}}(\boldsymbol{r}). \quad (11)\end{aligned}$$

$\varphi_\omega(\boldsymbol{r})$ is a scattering solution of equation (9). The result (11) provides the decomposition of the current into a one-body term describing the *elastic* channels, and a many-body term describing *inelastic* scattering.

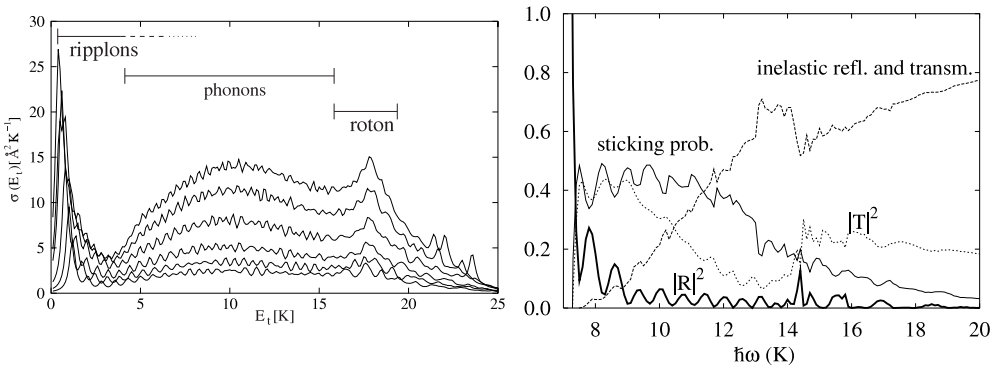

Figure 3. The left figure shows the cross-section for energy transfer $\sigma(E_t)$ for ^{3}He scattering at $^4\text{He}_N$ plotted as a function of E_t; the incident energy is $E = 26$ K and $N = 70, 112, 200, 400, 700, 1000$. Excitations of ripplons and rotons can be discerned, with a broad range of phonon excitations in between. The right figure shows the elastic reflectivity $|R|^2$ (thick curve), sticking probability, inelastic scattering probability, and transmittivity $|T|^2$ as a function of incident energy $\hbar\omega$ of ^{4}He atoms scattering from a ^{4}He slab of about 80 Å thickness. The probabilities add to unity.

Atom scattering calculations are relevant for two experimental activities: cluster scattering experiments; and quantum reflection and evaporation experiments. We have performed extensive calculations [7] on atom scattering off helium clusters; as an example, we show in figure 3(a) the cross-section for transferring energy from the impinging ^{3}He atom to the ^{4}He cluster. To model quantum reflection and evaporation experiments, we have studied symmetric slabs of ^{4}He with translational invariance in the x–y plane. Reflection and transmission probabilities are obtained by solving the effective Schrödinger equation (9) in this geometry, subject to the boundary conditions

$$\varphi_\omega(z) \to \begin{cases} \mathrm{e}^{\mathrm{i}k_\perp z} + R\mathrm{e}^{-\mathrm{i}k_\perp z} & \text{for } z \to -\infty \\ T\mathrm{e}^{\mathrm{i}k_\perp z} & \text{for } z \to \infty. \end{cases} \tag{12}$$

We consider normal incidence; the perpendicular wavevector, $k_\perp$, is then determined by the energy ω of the incident atom. If there is no energy loss, i.e. the single-particle excitations in the host liquid are non-interacting quasiparticles, then the single-particle flux is conserved and reflectivity and transmittivity add to unity: $|R|^2 + |T|^2 = 1$.

The fraction of inelastic scattering processes, i.e., sticking, inelastic reflectivity, or transmittivity, can be computed from the self-energy by keeping track of the decay channels of states excited by the impinging atom. An analysis of the asymptotic currents yields the combined probability for inelastic processes as

$$1 - |R|^2 - |T|^2 = -\frac{2m}{\hbar^2 k_\perp} \operatorname{Im} \int \mathrm{d}z\, \mathrm{d}z'\, \varphi^*_\omega(z) \Sigma(z, z'; \omega) \varphi_\omega(z'). \tag{13}$$

Figure 3(b) shows the probabilities of elastic and inelastic scattering processes as a function of the incident energy $\hbar\omega$ in the case of scattering from a helium slab. The oscillations in the elastic and inelastic scattering probabilities in figure 3(b) arise as a consequence of the finite thickness of the slab. The result shows quantum reflection at very low energies; at slightly higher energies sticking is the dominant process due to low-energy ripplon modes on the surface. The peaky structure near 14 K is due to roton excitation; experimentally, we expect these features to show up at slightly lower energies, because the excitation energies in the roton region are overestimated by the present theory.

Acknowledgments

This work was supported, in part, by the Austrian Science Fund under project P-12832-TPH. One of us (EK) thanks the Institute for Nuclear Theory at the University of Washington for hospitality and the US Department of Energy for partial support.

References

[1] Krotscheck E and Navarro J 2002 *Microscopic Approaches to Quantum Liquids in Confined Geometries* (Singapore: World Scientific)
[2] Apaja V and Krotscheck E 2002 *Microscopic Approaches to Quantum Liquids in Confined Geometries* ed E Krotscheck and J Navarro (Singapore: World Scientific) pp 205–68
[3] Clements B E, Krotscheck E and Lauter H J 1993 *Phys. Rev. Lett.* **70** 1287
[4] Apaja V and Krotscheck E 2001 *J. Low Temp. Phys.* **123** 241
[5] Chin S A and Krotscheck E 1992 *Phys. Rev.* B **45** 852
[6] Lauter H J, Godfrin H and Wiechert H 1985 *Proc. 2nd Int. Conf. on Phonon Physics* ed J Kollàr, N Kroo, M Meynhard and T Siklos (Singapore: World Scientific) p 842
[7] Krotscheck E and Zillich R 2001 *J. Chem. Phys.* **22** 10161